Surface Tomonaga-Luttinger-Liquid State on Bi/InSb(001)

Yoshiyuki Ohtsubo,[1,2,3,*] Jun-ichiro Kishi,[2] Kenta Hagiwara,[2] Patrick Le Fèvre,[3] François Bertran,[3]
Amina Taleb-Ibrahimi,[3,4] Hiroyuki Yamane,[5] Shin-ichiro Ideta,[5] Masaharu Matsunami,[5]
Kiyohisa Tanaka,[5] and Shin-ichi Kimura[1,2,†]

[1]*Graduate School of Frontier Biosciences, Osaka University, Suita 565-0871, Japan*
[2]*Department of Physics, Graduate School of Science, Osaka Unviersity, Toyonaka 560-0043, Japan*
[3]*Synchrotron SOLEIL, Saint-Aubin-BP 48, F-91192 Gif sur Yvette, France*
[4]*UR1/CNRS Synchrotron SOLEIL, Saint-Aubin, F-91192 Gif sur Yvette, France*
[5]*Institute for Molecular Science, Okazaki 444-8585, Japan*
(Received 15 April 2015; revised manuscript received 19 August 2015; published 17 December 2015)

A 1D metallic surface state was created on an anisotropic InSb(001) surface covered with Bi. Angle-resolved photoelectron spectroscopy (ARPES) showed a 1D Fermi contour with almost no 2D distortion. Close to the Fermi level (E_F), the angle-integrated photoelectron spectra showed power-law scaling with the binding energy and temperature. The ARPES plot above E_F, obtained thanks to a thermally broadened Fermi edge at room temperature, showed a 1D state with continuous metallic dispersion across E_F and power-law intensity suppression around E_F. These results strongly suggest a Tomonaga-Luttinger liquid on the Bi/InSb(001) surface.

The Fermi liquid theory of ordinal three-dimensional (3D) metals breaks down in one-dimensional (1D) systems to produce various exotic quantum phases. Tomonaga-Luttinger liquid (TLL) [1,2] is an exactly solvable model of a gapless 1D quantum system that is characterized by power-law scaling and spin-charge separation for low-energy excitation spectra [3]. So far, various 1D systems have been studied as TLL candidates. Only a few have shown metallic states with power-law spectral features, e.g., carbon nanotubes [4] and lithium purple bronze [5,6]. The other characteristic of spin-charge separation has been reported in some 3D materials with 1D electronic structures [7–9].

The surface of semiconductors is known to show various self-assembled 1D atomic structures that are regarded as suitable systems for studying 1D metallic states [10,11], such as In/Si(111) [12], Au/Si(557) [13], and Pt/Ge(001) [14]. On such surface systems, *in situ* electron or hole doping can be performed by the deposition of additional atoms, and the local atomic structure can be observed or controlled by scanning probe techniques. These manipulations on the surface 1D states can provide further insight into 1D physics. Hence, surface TLLs have attracted much attention in the past two decades. However, despite the various 1D surfaces, most of them do not behave as TLLs at low temperature. Possible reasons for the non-TLL behavior have been discussed for each specific system, such as a metal-insulator transition at low temperatures [15] and interaction with other two-dimensional (2D) surface bands [16].

So far, the only candidate for a surface TLL is an Au nanowire assembled on Ge(001) [Au/Ge(001)], which shows power-law scaling for low-energy spectral features

according to scanning tunneling spectroscopy (STS) and angle-resolved photoelectron spectroscopy (ARPES) [17,18]. However, a recent work presented doubt with regard to the TLL picture and proposed an alternative interpretation of the STS spectra: two different and gapped states lying just above or below the Fermi level (E_F) [19]. This picture can also explain the STS spectral shape around E_F. In order to distinguish these two possibilities without ambiguity, the 1D band dispersion needs to be traced across E_F continuously with k resolution in reciprocal space. However, to the best of our knowledge, no such experimental data have been reported about surface TLLs so far. While some ARPES results have been given for Au/Ge(001) [17,18,20], the dispersion above E_F is not accessible with these data.

In this Letter, we report on the case of a new surface TLL candidate discovered with ARPES on a Bi-induced anisotropic structure on InSb(001) [Bi/InSb(001)]. The Bi/InSb(001) surface state (SS) showed a 1D Fermi contour (FC) with almost no undulation and stayed metallic down to 35 K. The 1D feature is the unique contour on E_F of the sample, which showed a parabolic dispersion with its bottom at the center of the surface Brillouin zone (SBZ). The photoelectron spectra in the proximity of E_F obey power-law scaling as a function of binding energy and sample temperature with the same power index $\alpha = 0.7 \pm 0.1$. The ARPES plot divided by the Fermi distribution function at room temperature (RT) indicated the 1D state with continuous metallic dispersion across E_F and power-law intensity suppression around E_F. These results strongly suggest that the 1D surface structure of Bi/InSb(001) hosts a surface TLL.

The Bi/InSb(001) surface was prepared by evaporating three monolayers of Bi on the clean surface of InSb(001) substrates (*n*-type, carrier concentration of 2×10^{14} cm^{-3}) and a subsequent flash by direct current heating up to 680 K for ~ 10 sec. After the preparation, the $p(1 \times 3)$ surface periodicity was observed by low-energy electron diffraction [Fig. 1(a)]. The detailed procedure on sample preparation and characterization, especially the comparison with the $c(2 \times 6)$ surface reported in a previous work [21], is shown in the Supplemental Material [22].

Figures 1(c–e) indicate the surface electronic structure of Bi/InSb(001) measured with ARPES. ARPES measurements were performed with a He lamp and synchrotron radiations at the CASSIOPÉE beamline of synchrotron SOLEIL and BL7U of UVSOR-III. The photon energies used ranged from 12 to 40.8 eV. The photoelectron kinetic energy at E_F and the overall energy resolution of each
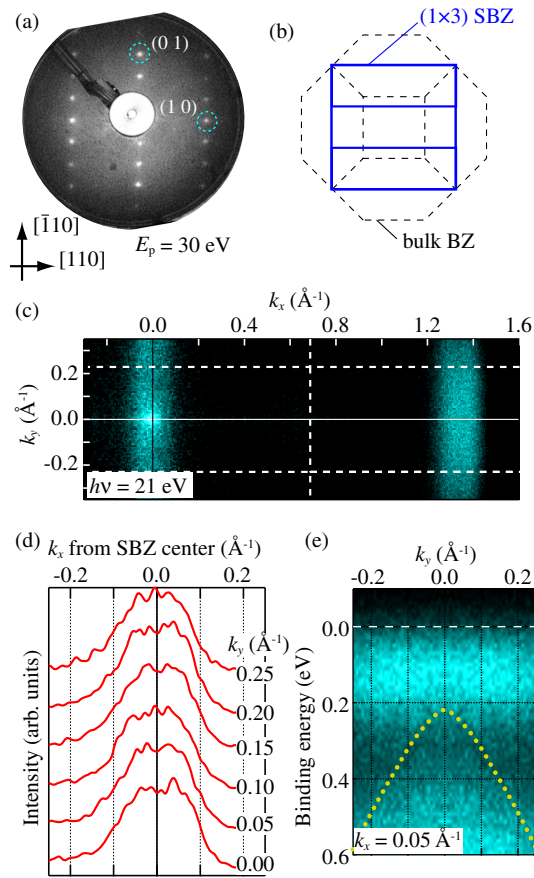

(a) [LEED pattern with labels (0 1), (1 0), $[\bar{1}10]$, [110], $E_p = 30$ eV]

(b) [(1×3) SBZ, bulk BZ]

(c) k_x (Å^{-1}) / k_y (Å^{-1}), $h\nu = 21$ eV

(d) k_x from SBZ center (Å^{-1}), Intensity (arb. units), k_y (Å^{-1}): 0.25, 0.20, 0.15, 0.10, 0.05, 0.00

(e) k_y (Å^{-1}), Binding energy (eV), $k_x = 0.05$ Å^{-1}

FIG. 1 (color online). (a) Low-energy electron diffraction patterns of Bi/InSb(001)-(1 × 3) taken at room temperature (RT). (b) Surface and bulk Brillouin zones of Bi/InSb(001). (c)–(e) ARPES results at RT measured with $h\nu = 21$ eV. (c) Constant energy contour around the Fermi level (E_F). The dashed lines indicate boundaries of the surface Brillouin zone (SBZ). k_x and k_y are defined parallel and perpendicular, respectively, to [110]. ARPES intensities are integrated over 20 meV windows centered at E_F. (d) Momentum distribution curves in second SBZ. (e) Band dispersion around E_F along k_y.

ARPES setup were carefully calibrated by the Fermi edge of the photoelectron spectra from freshly evaporated gold on the sample after the measurement [see Fig. 3(a)].

Figure 1(c) shows the Fermi contour (FC) around E_F as measured with linearly polarized photons. k_x and k_y are defined to be parallel to [110] and [$\bar{1}$10], respectively. The linear shape of the FC along k_y clearly indicated a 1D metallic state on the surface. Such a 1D FC is consistent with the anisotropic (1 × 3) surface periodicity indicated by LEED. The dispersion of the 1D state did not change with the photon energy (shown in the Supplemental Material [22]), which indicates no dispersion along k_z as would be expected for a surface state. Figure 1(c) also shows that there were no other metallic states on the surface. Therefore, this FC provides a unique and highly anisotropic conduction path on the surface. As shown in Fig. 1(d), the ARPES momentum distribution curves (MDCs) indicated that the SS was exactly 1D without any 2D distortion. MDCs were captured in the second SBZ because the SS dispersion became clearer there owing to the photoexcitation matrix element effect. The lack of 2D distortion can also be observed in the E-k_y plot in Fig. 1(e). The dotted curve is the upper edge of the projected bulk valence bands as calculated according to Ref. [24]. The bulk valence band maximum position was determined with the linear method (see the Supplemental Material for details [22]).

Note that the 1D FC appeared with a single domain, in contrast to the double-domain case of Au/Ge(001) [18], where the direction of the conduction path is still under debate because of the two equivalent domains rotated 90° with each other [19,25]. This is because of the reduced symmetry of the zinc blende crystal structure compared to group-IV semiconductors. Along the [001] direction, a III-V semiconductor lattice is stacked alternately with group III and V atoms (indium and antimony for InSb). Hence, the equivalent plane appears at every two atomic steps on the (001) surface of such crystal. In the group IV semiconductor crystal, every atomic plane along [001] is equivalent and appears with 90° rotation at each atomic step to form the double-domain surface structure. The 90° rotation at each atomic step also occurs for III-V semiconductors; the double atomic step results in a 180° rotation, so the steps are actually identical thanks to the twofold rotation symmetry. Thus, the conduction path of the Bi/InSb(001) surface was clearly demonstrated to be parallel to [110].

Figure 2 shows the dispersion of the surface band on Bi/InSb(001). The surface state formed a single parabolic band with its bottom at $k_x = 0$ Å^{-1}. This band is the unique metallic feature on the surface. This 1D metallic band crossed E_F only once on each side of the SBZ. At higher binding energies, the bottom of the surface-state band showed a small shift (~ 50 meV) between $k_y = 0.0$ and 0.2 Å^{-1}. This would be due to an overlap of the bulk valence bands. The dotted (solid) curves in Fig. 2 are the
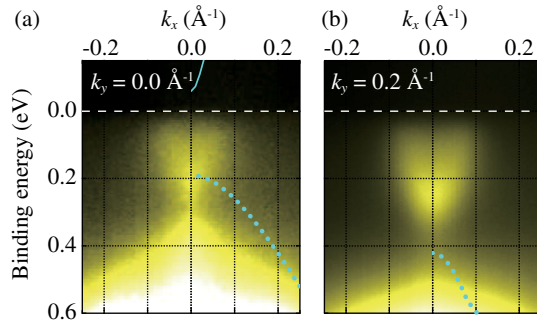
FIG. 2 (color online). (a),(b) Band dispersions along k_y at 8 K with $h\nu = 15$ eV. The dotted (solid) curves represent the upper (lower) edges of projected bulk valence (conduction) bands.

upper (lower) edges of the projected bulk valence (con-duction) bands and were calculated in the same manner as those in Fig. 1(e). The bottom of the SS overlapped the bulk valence bands at the center of the SBZ. Note that the bulk conduction band does not cross E_F, as shown by the solid curve in Fig. 2(a).

In order to examine the 1D nature of the surface state, we compared the angle-integrated photoelectron spectrum with that from ordinary metal (Au evaporated on the sample after the ARPES measurement), as shown in Fig. 3(a). The angle integration was performed at $k_y = 0.25 \pm 0.05$ Å^{-1}. Figure 3(a) clearly shows the suppression of the photo-electron intensity at E_F compared to that from Au, which suggests a deviation of the surface state from the Fermi-liquid framework. We tried to fit the spectrum to the TLL spectral function considering the finite temperature, as given in some of the literature [26,27]. Based on Ref. [26], the spectral function of the angle-integrated PES can be written as

$$I(\epsilon, T) \propto T^\alpha \cosh\left(\frac{\epsilon}{2}\right) \left| \Gamma\left(\frac{1+\alpha}{2} + i\frac{\epsilon}{2\pi}\right) \right|^2 f(\epsilon, T), \quad (1)$$

where $\epsilon = E/k_B T$ is the temperature-normalized energy, Γ is the gamma function, and $f(\epsilon, T) = (e^\epsilon + 1)^{-1}$ is the Fermi distribution function. When convolved with the Gaussian instrumental energy resolution ($\Delta E = 10$ meV), this function reproduced the spectra well at 35 K [Fig. 3(a)] with $\alpha = 0.65 \pm 0.05$ in the low-energy region. This func-tion only fits the spectrum below 0.1 eV. This was because the TLL framework is only valid in the proximity of E_F (see the Supplemental Material for detailed analysis [22]).

The power-law scaling of a TLL should show a universal power index with various parameters. Figures 3(b) and 3(c) show the temperature dependence of the photoelectron intensities at E_F. The intensity from 180 to 50 K decreased linearly with log T, which indicates power-law scaling of the spectral intensities, $I_{E=E_F}(T) \propto T^\alpha$. The slight change in the slope below 50 K was due to the finite ΔE. This broadening was already convolved in the fitting curve (blue solid line) to give a power index of $\alpha = 0.71 \pm 0.10$, which
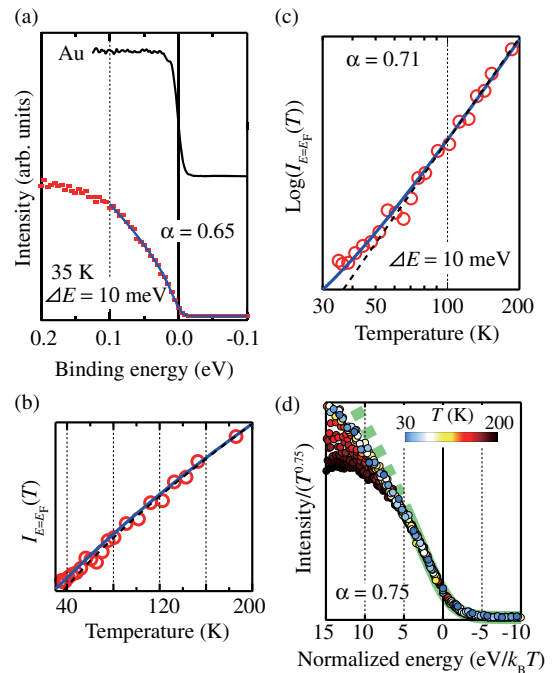

FIG. 3 (color online). (a) Photoelectron spectrum (red markers) integrated along k_x ($k_y = 0.25 \pm 0.05$ Å^{-1}). The solid line between ± 0.1 eV is the fitting curve (see text for details). (b) Temperature dependence of the photoelectron intensity at E_F [$I_{E=E_F}(T)$]. Each spectrum was normalized at the intensity at 0.2 eV below E_F in order to compensate for the sample degradation. The solid (blue) line is the fitting curve based on power-law scaling ($T^{0.71}$) convolved with ΔE (10 meV). The dashed line is $T^{0.73}$ without broadening from ΔE. (c) The same as (b) plotted in a log scale. (d) Universal scaling plot of the spectra at various temperatures, using a T-renormalized energy scale (eV/$k_B T$). The thick dotted (green) line is from Eq. (1) with the scaling factor $\alpha = 0.75$.

is a value very close to that obtained by fitting the energy scale [Fig. 3(a)]. Note that $I_{E=E_F}(T)$ should be constant in the case of a Fermi-Dirac system.

Another method to examine universal power-law scaling is to normalize the spectra taken at various temperatures to T^α and plot them versus the temperature-normalized energy ϵ, as shown in Fig. 3(d). With such a renormalization, all spectra with various T become almost identical in the low-energy region, typically in $\epsilon \leq 5$. For such identifica-tion, the scaling factor $\alpha = 0.75 \pm 0.05$ is required (spectra renormalized with another α are shown in the Supplemental Material [22]). Because such a temperature normalization method can include the intensity not only at $E = E_F$ but within the finite energy window, this renormalized plot would be the best way to estimate the power index from angle-integrated spectra taken at various temperatures. All of these spectral features indicate that the 1D surface state on Bi/InSb(001) obeys a universal power-law scaling with $\alpha = 0.7 \pm 0.1$, which agrees with that expected for a TLL.

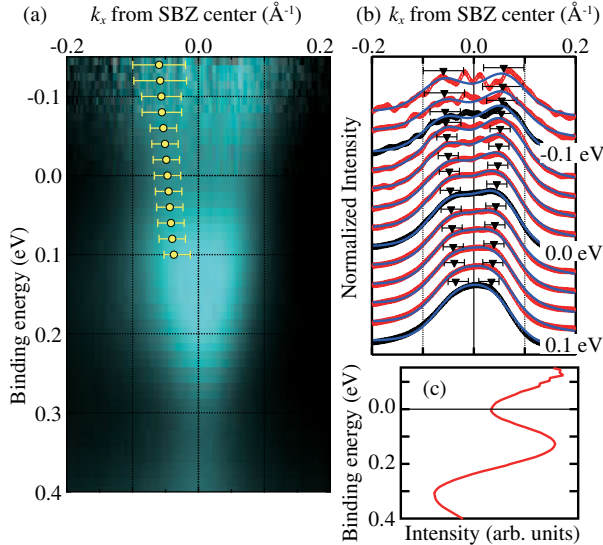(a) k_x from SBZ center (Å⁻¹) (b) k_x from SBZ center (Å⁻¹)

FIG. 4 (color online). (a) ARPES intensity plot along k_x divided by the Fermi distribution function convolved with the instrumental resolution taken at $h\nu = 21$ eV. ARPES data were integrated along k_y within $|k_y| < 0.3$ Å⁻¹ for better statistics. (b) ARPES MDCs along k_x within a 20 meV energy window. The intensities of each curve were normalized by the peak height. Solid lines are the fitting curves (see text for details). (c) An angle-integrated EDC within $|k_x| < 0.3$ Å⁻¹ divided by the Fermi distribution function, similar to (a).

To obtain further insight into the 1D SS, we looked into the detailed structure of ARPES spectra. Figure 4(a) shows the ARPES intensity plot at RT along k_x divided by the Fermi distribution function convolved with the instrumental resolution. For better statistics, the ARPES plot was integrated along k_y within $|k_y| < 0.3$ Å⁻¹. The momentum distribution curves (MDCs) are shown in Fig. 4(b). They are fitted well by a pair of Voigt peaks (Gaussian and Lorentzian widths are fixed for every peak) and linear backgrounds [solid lines in Fig. 4(b)]. Weak residuals around $k_x = 0$ Å⁻¹ at the binding energies below -0.1 eV would be due to the bulk conduction bands. From the MDCs, we obtained the peak positions at each binding energy and overlaid them on Fig. 4(a). They indicated the Fermi wave vector $|k_F|$ to be 0.05 ± 0.02 Å⁻¹. This estimation is consistent with the ARPES data taken at low temperature shown in Fig. 2. This shows the continuous, metallic dispersion of the 1D SS across E_F. Moreover, the ARPES intensity plot clearly shows that the spectral intensity of the 1D SS was suppressed around E_F, without breaking the continuity of the band dispersion. Such suppression of the density of states (DOS) around E_F without any gap opening reflects the power-law scaling of the TLL. This result excludes alternative possibilities without ambiguity. Two different states below or above E_F cannot reproduce such a dispersion. In addition, the angle-integrated spectrum showed a temperature-broadened power-law shape for the density of states around E_F, as expected in theory [26]. At RT, it sometimes becomes

difficult to determine the exact position of E_F because of the broad Fermi edge. However, note that such ambiguity did not affect the DOS suppression obtained by ARPES: the intensity suppression appeared irrespective of slight artificial shifts in E_F.

In summary, a new candidate for a surface TLL formed on Bi/InSb(001) has been discovered. A surface state formed a 1D FC with almost no 2D undulation and stayed metallic down to 35 K. This 1D FC is the only metallic feature of the sample and hence provides a unique 1D conduction path on the surface. The photoelectron spectra in the proximity of E_F obeyed the power-law scaling as a function of binding energy and sample temperature with the same power index $\alpha = 0.7 \pm 0.1$. Moreover, the ARPES plot above E_F obtained thanks to the thermally broadened Fermi edge at RT indicated a 1D state with continuous metallic dispersion across E_F and power-law intensity suppression around E_F. These results strongly suggest that the 1D surface structure Bi/InSb(001) hosts a surface TLL. The new 1D SS on Bi/InSb(001) would provide a fertile playground for further studies of low-dimensional physics.

*y_oh@fbs.osaka-u.ac.jp
†kimura@fbs.osaka-u.ac.jp

[1] S. Tomonaga, Prog. Theor. Phys. **5**, 544 (1950).
[2] J. M. Luttinger, J. Math. Phys. (N.Y.) **4**, 1154 (1963).
[3] J. Voit, Rep. Prog. Phys. **58**, 977 (1995).
[4] H. Ishii et al., Nature (London) **426**, 540 (2003).
[5] F. Wang, J. V. Alvarez, S.-K. Mo, J. W. Allen, G.-H. Gweon, J. He, R. Jin, D. Mandrus, and H. Höchst, Phys. Rev. Lett. **96**, 196403 (2006).
[6] L. Dudy, J. D Denlinger, J. W. Allen, F. Wang, J. He, D. Hitchcock, A. Sekiyama, and S. Suga, J. Phys. Condens. Matter **25**, 014007 (2013).
[7] R. Claessen, M. Sing, U. Schwingenschlögl, P. Blaha, M. Dressel, and C. S. Jacobsen, Phys. Rev. Lett. **88**, 096402 (2002).
[8] B. J. Kim et al., Nat. Phys. **2**, 397 (2006).
[9] Y. Jompol, C. J. B. Ford, J. P. Griffiths, I. Farrer, G. A. C. Jones, D. Anderson, D. A. Ritchie, T. W. Silk, and A. J. Schofield, Science **325**, 597 (2009).
[10] F. J. Himpsel, K. N. Altmann, R. Bennewitz, J. N. Crain, A. Kirakosian, J.-L. Lin, and J. L. McChesney, J. Phys. Condens. Matter **13**, 11097 (2001).
[11] M. Grioni, S. Pons, and E. Frantzeskakis, J. Phys. Condens. Matter **21**, 023201 (2009).

[12] J. Nogami, S. I. Park, and C. F. Quate, Phys. Rev. B **36**, 6221 (1987).

[13] P. Segovia, D. Purdie, M. Hengsberger, and Y. Baer, Nature (London) **402**, 504 (1999).

[14] O. Gurlu, O. A. O. Adam, H. J. W. Zandvliet, and B. Poelsema, Appl. Phys. Lett. **83**, 4610 (2003).

[15] H. W. Yeom *et al.*, Phys. Rev. Lett. **82**, 4898 (1999).

[16] K. Yaji *et al.*, Phys. Rev. B **87**, 241413(R) (2013).

[17] C. Blumenstein, J. Schäfer, S. Mietke, S. Meyer, A. Dollinger, M. Lochner, X. Y. Cui, L. Patthey, R. Matzdorf, and R. Claessen, Nat. Phys. **7**, 776 (2011).

[18] S. Meyer, L. Dudy, J. Schäfer, C. Blumenstein, P. Höpfner, T. E. Umbach, A. Dollinger, X. Y. Cui, L. Patthey, and R. Claessen, Phys. Rev. B **90**, 125409 (2014).

[19] J. Park, K. Nakatsuji, T.-H. Kim, S. K. Song, F. Komori, and H. W. Yeom, Phys. Rev. B **90**, 165410 (2014).

[20] K. Nakatsuji, Y. Motomura, R. Niikura, and F. Komori, Phys. Rev. B **84**, 115411 (2011).

[21] P. Laukkanen *et al.*, Phys. Rev. B **81**, 035310 (2010).

[22] See Supplemental Material at http://link.aps.org/supplemental/10.1103/PhysRevLett.115.256404 for the detailed sample preparation procedure, additional ARPES dataset, and detailed analysis of the spectra based on the TLL model, which includes Refs. [21,23].

[23] S. A. Chambers, T. Droubay, T. C. Kaspar, and M. Gutowski, J. Vac. Sci. Technol. B **22**, 2205 (2004).

[24] D. J. Chadi, Phys. Rev. B **16**, 790 (1977).

[25] K. Nakatsuji and F. Komori, Nat. Phys. **8**, 174 (2012).

[26] K. Schönhammer and V. Meden, J. Electron Spectrosc. Relat. Phenom. **62**, 225 (1993).

[27] D. Orgad, Philos. Mag. B **81**, 377 (2001).